Experimental evidence for dissipationless transport of the chiral edge state of the high-field Chern insulator in $MnBi_2Te_4$ nanodevices

Zhe Ying,[1,*] Shuai Zhang,[1,*,†] Bo Chen,[1,*] Bin Jia,[1] Fucong Fei,[1,‡] Minhao Zhang,[1] Haijun Zhang,[1] Xuefeng Wang,[2] and Fengqi Song[1,§]

[1]*National Laboratory of Solid State Microstructures, Collaborative Innovation Center of Advanced Microstructures, and School of Physics, Nanjing University, Nanjing 210093, China*

[2]*National Laboratory of Solid State Microstructures, Collaborative Innovation Center of Advanced Microstructures, and School of Electronic Science and Engineering, Nanjing University, Nanjing 210093, China*

(Received 23 February 2021; revised 7 August 2021; accepted 26 January 2022; published 14 February 2022)

We study the dissipationless transport properties of chiral edge state (CES) in the Chern insulator $MnBi_2Te_4$ devices. A near-zero longitudinal resistance and a quantized Hall plateau $\sim 0.97 h/e^2$ up to 22 K are observed. The CES shows three regimes of temperature dependence, i.e., well-preserved dissipationless transport below 6 K, variable range hopping (6 $\sim$ 22 K) and thermal activation (>22 K). This indicates nondissipation as well as the chirality of the edge state, in conjunction with the nonlocal measurements. At 2 K, a current of over 1.4 μA could break the dissipationless transport. Besides, it is found that a *p-n* junction has almost no influence upon the CES of Chern insulator $MnBi_2Te_4$. These present a comprehensive picture of the CES transport in this newly emerging material.

DOI: 10.1103/PhysRevB.105.085412

The Hall resistance can be quantized without the formation of the Landau level (LL), which is the case of quantum anomalous Hall effect (QAHE) and also known as the Chern insulator state [1]. Driven by the coexistence of nontrivial topology of the electronic structure and ferromagnetism exchange, the long-desired QAHE was first observed in the magnetically doped topological insulator (TI) Cr-$(Bi, Sb)_2Te_3$ [2]. However, inhomogeneity due to the presence of magnetic dopants may lead to a rather small effective magnetic exchange gap, and thus the QAHE onset temperature in a magnetically doped TI is still below 2 K, despite considerable efforts having been devoted [3–5]. $MnBi_2Te_4$ was predicted and experimentally verified to be an intrinsic magnetic TI [6–18], where the magnetism originates from long-range ordered Mn atoms, rather than stochastically distributed dopants in previous systems. Thus, it becomes a promising platform to explore QAHE and Chern insulator state at higher temperature, as observed in recent experiments in flakes of $MnBi_2Te_4$ [19–22]. Even the interesting axion insulator [22] and high Chern number state [21] can be simulated. Research enthusiasm is ignited afterwards on the family of $MnBi_2Te_4$.

Besides the quantized Hall plateaus, dissipationless CES transport deserves investigation and should be demonstrated to form a complete set of evidence of Chern insulator state. However, this has been rarely studied and still lacks particularly in satisfactory devices with consistent temperature dependence between the CES and Hall plateau. Here, we demonstrate the dissipationless transport of the CES in the Chern insulator $MnBi_2Te_4$ devices. The well-defined quantization can survive up to 22 K, with the Hall plateau $\sim 0.97\, h/e^2$, where h is the Planck constant and e is the electron charge. The temperature-dependent CES transport are explored by both the local and nonlocal measurements, which reveals the transition from well-preserved dissipationless state to variable range hopping (VRH) and thermal activation. We also investigate the current dependence of the CES transport [23–28], which is of great importance for future applications. Finally, the effect of a *p-n* junction on the Chern insulator has been explored as well.

The $MnBi_2Te_4$ crystal was grown using the flux method [13]. After mechanical exfoliation and microfabrication, a $MnBi_2Te_4$ field-effect transistor was obtained [29]. A hexagonal boron nitride (BN) flake was transferred to the top of the device to protect the $MnBi_2Te_4$ sample, as shown in Fig. 1(a). Our first device (labeled as M3, hereafter) is a five septuple-layers (SLs) $MnBi_2Te_4$ [inset of Fig. 1(c)].

Figure 1(b) is the zero-field mapping of R_{xx} as a function of back-gate voltage (V_{bg}) and temperature (T). The ambipolar behavior of R_{xx} (V_{bg}) can be found [also see Fig. 2(a)], which indicates that the charge neutral point (CNP) is reachable. It provides the opportunity to observe the Chern insulator state. Figure 1(c) shows the CNP resistance (R_{CNP}) versus temperature extracted from Fig. 1(b). The clear kink around 22 K indicates the Néel temperature (T_N) of M3. It is a little bit lower than that of the bulk crystal ($\sim$ 25 K) because of the thermal fluctuations as the sample approaches two-dimension limit [19,30]. Around Néel temperature, R_{CNP} is extremely large, at more than 100 kΩ.

Near the CNP, the Chern insulator state is observed. In Fig. 1(d), $V_{bg} = 47$ V, R_{xx} is almost zero at high magnetic field

*These authors contributed equally to this work.
†Corresponding author: szhang@nju.edu.cn
‡Corresponding author: feifucong@nju.edu.cn
§Corresponding author: songfengqi@nju.edu.cn

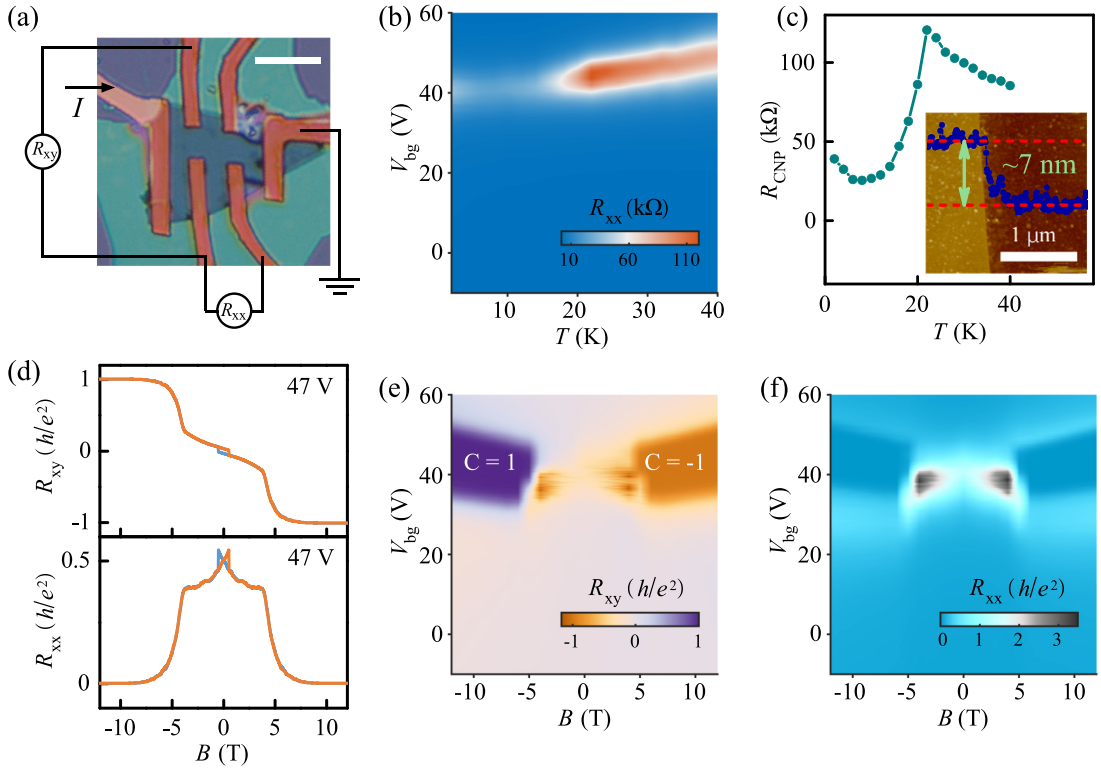

FIG. 1. Observation of the Chern insulator state in $MnBi_2Te_4$ thin flakes. (a) Optical micrograph of M3 in the main text and our measurement configuration. Scale bar, 10 μm. (b) Color map of R_{xx} as a function of gate voltage and temperature at zero field. (c) The resistance of the charge neutral point (R_{CNP}) extracted from (b) exhibits a kink around 22 K. The inset is the topography image by atomic force microscope. (d) At 1.7 K, when the Fermi level is tuned close to the CNP, the Chern insulator state can be observed. (e) R_{xy} mapping as a function of V_{bg} and B at 1.7 K without antisymmetrization. (f) The corresponding R_{xx} mapping without symmetrization.

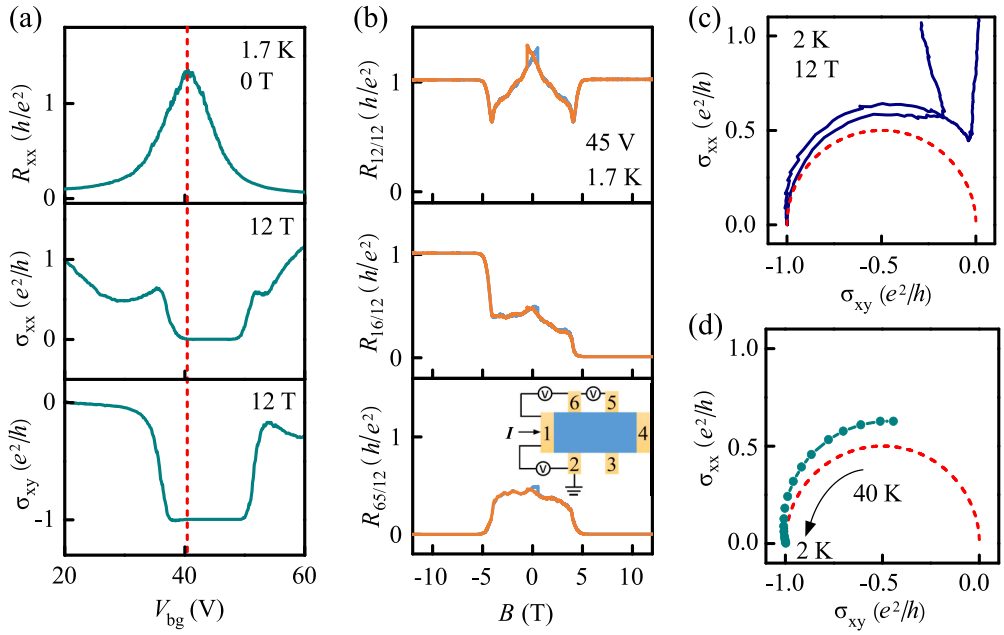

FIG. 2. The features of Chern insulator state. (a) The zero-field R_{xx} and high-field σ_{xx} and σ_{xy}, from top to bottom. The CNP is located within the -1 plateau. (b) The magnetoresistance of $R_{12/12}$, $R_{16/12}$, $R_{65/12}$ at $V_{bg} = 45$ V, from top to bottom. The inset defines the probe numbers. (c) The renormalized group flow. (d) The converging points extracted from renormalized group flow at 12 T for different temperatures.

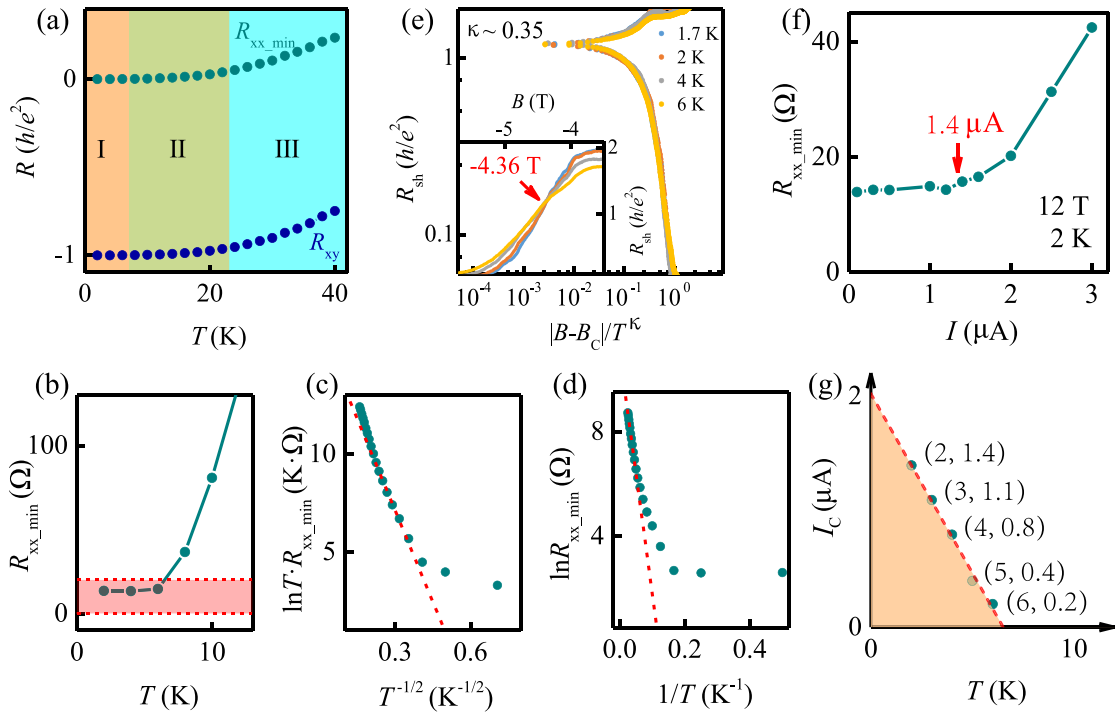

FIG. 3. The scaling behaviors of the Chern insulator state. (a) The temperature-dependent R_{xx} minimum (R_{xx_min}) and R_{xy} at 12 T. (b) The well-developed dissipationless CES below 6 K, with R_{xx_min} around 14 Ω. (c) The VRH fitting. (d) The thermal activation fitting. (e) The scaling analysis in the vicinity of a critical magnetic field ~ –4.36 T. (f) The current-induced breakdown of the dissipationless CES, with a critical current ~1.4 μA. (g) The temperature-dependent critical current measured at 12 T.

(B), and the Hall resistance $R_{xy}(= V_{26}/I_{14})$ is well quantized (see Fig. S2 in Supplemental Material [31] for more magneto-transport at various V_{bg}). The V_{bg}-dependent R_{xy} and R_{xx} with B changing from +12 T to −12 T is shown in Figs. 1(e) and 1(f), respectively. It can be found that the quantization appears when $|B| \geqslant 6$ T, which can effectively polarize $MnBi_2Te_4$ thin films from antiferromagnetic (AFM) to ferromagnetic (FM) state. In the thick $MnBi_2Te_4$ flakes, the transition field from FM to AFM is ~ 7.7 T (Supplemental Material, Fig. S1 [31]). It might be the dimensional effect that the polarization field in the thin film (~ 6T, here) is smaller than that in the bulk crystal [16,32].

In Fig. 2(a), V_{bg}-dependent zero-field R_{xx} and high-field ($B = 12$ T) σ_{xx} and σ_{xy} are shown. Obviously, the CNP is located within the quantization regime. This means that the quantization plateau retains its sign in both the n- and p-type carrier regions, which rules out the possibility of QHE with LL. To verify the dissipationless CES, the two-probe resistance $R_{12/12}$ $(= V_{12}/I_{12})$, three-probe resistance $R_{16/12}$ $(= V_{16}/I_{12})$, and nonlocal four-probe resistance $R_{65/12}$ $(= V_{65}/I_{12})$ are shown in Fig. 2(b). The $R_{12/12}$ always exhibits a plateau of $+1\,h/e^2$ at both positive and negative magnetic field when it settles into the quantization regime, and $R_{65/12}$ is always near zero. It is the direct feature of the CES of a Chern insulator. Differently, $R_{16/12}$ is $+1\,h/e^2$ in the negative magnetic field, and zero in the positive field, which can be explained by the Landauer-Büttiker formalism [33,34]. In a positive magnetic field, clockwise channel chirality is expected, and the voltage potentials are $V_1 = V_6 = V_5 = V_4 = V_3$, thus V_{16} should be equal to V_{65}, which is zero. Therefore, $R_{16/12} = R_{65/12} = 0$. In a negative magnetic field, however, the voltage potentials are $V_6 = V_5 = V_4 = V_3 = V_2$, thus V_{16} should be equal to V_{12}, showing $R_{16/12} = R_{12/12} = +1\,h/e^2$. The chirality of the edge state is thus shown convincingly.

The temperature-dependent Chern insulator state at $B = 12$ T is shown in Fig. S4 (Supplemental Material [31]), and the quantization regime in the mapping shrinks with increasing temperature. The Fermi-level-derived renormalized group (RG) flow [35,36] in the (σ_{xy}, σ_{xx}) space at 12 T and 2 K is shown in Fig. 2(c). We find that it satisfies the semicircular scaling law (indicated by the dashed red line) very well. The temperature-dependent converging point extracted from the RG flow is shown in Fig. 2(d), which flows to $(-1\,e^2/h, 0)$ with decreasing temperature. The temperature- and Fermi-level-dependent RG flow provide a good description of the Chern insulator state.

In Fig. 3(a), the temperature-dependent R_{xx} minimum (R_{xx_min}) and R_{xy} plateau in the quantization regime are shown (extracted from Fig. S4 in Supplemental Material [31]). Below 22 K, the quantization value of $|R_{xy}|$ is larger than $0.97\,h/e^2$, and the R_{xx_min} is less than $0.04\,h/e^2$. This is adopted as an indication of the quantization criterion. Interestingly, we note that the temperature can be divided into three regimes. When $T \leqslant 6$ K (regime I), R_{xx_min} is around 14 Ω, and it remains unchanged as indicated by the pink box in Fig. 3(b). Such a small value of R_{xx_min} is a hallmark of the well-preserved dissipationless CES transport. When $T > 6$ K, R_{xx_min} increases sharply, which implies the breakdown of the dissipationless CES. When 6 K $< T <$ 22 K (regime II), R_{xx_min} changes from 36 to 1006 Ω. The linear relationship between $\ln T\cdot$

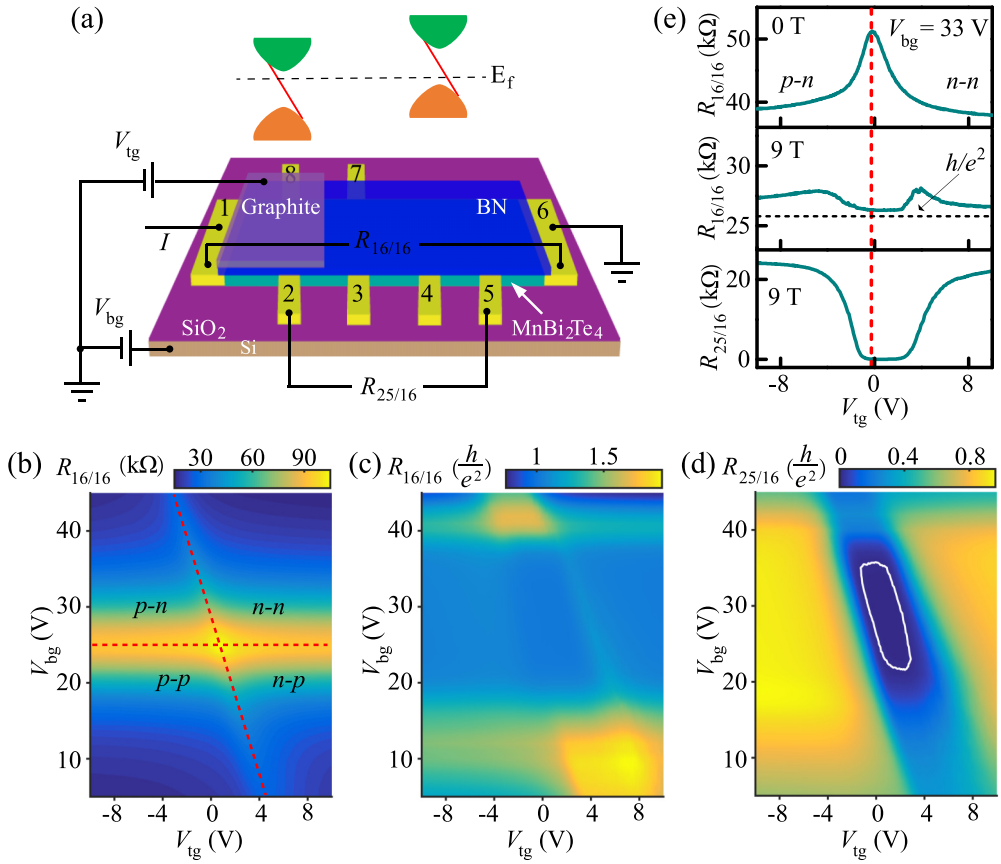

FIG. 4. The *p-n* junction in the Chern insulator state (M6). (a) The measurement configuration of the *p-n* junction device (M6 in the main text). (b) The dual-gate-dependent $R_{16/16}$ mapping at $B = 0$ T. The dashed lines separate the *p-n*, *p-p*, *n-p*, and *n-n* regions. (c), (d) The dual-gate-dependent $R_{16/16}$ and $R_{25/16}$ at $B = 9$ T. The white circle encloses the region where $R_{25/16} < 0.01\,h/e^2$. (e) $R_{16/16}$ ($B = 0$ T), $R_{16/16}$ ($B = 9$ T), and $R_{25/16}$ ($B = 9$ T) vs V_{tg}, which are line-cut profiles from (b), (c), and (d) with $V_{bg} = 33$ V, respectively. The temperature is 1.7 K.

R_{xx_min} and $T^{-1/2}$ in this regime [the dashed red line in Fig. 3(c)] indicates that the transport behavior can be described by VRH [23,37,38]. When $T > 22$ K (regime III), an Arrhenius plot with $R_{xx\_min} \propto \exp(-T_0/T)$ reveals the thermal activation behavior [Fig. 3(d)], where $T_0 = \Delta E/2k_B$, ΔE is the thermal activation gap, and k_B is the Boltzmann constant. The extracted gap is $T_0 \sim 92$ K. Although the transition temperature from VRH to thermal activation is ~22 K, which seems to be consistent with the Néel temperature, we should note that this is more like a coincidence for there are no noticeable features near 22 K in Fig. 3(a), being different from Fig. 1(c). As it is polarized FM state at high field, the Néel temperature would have no significant contribution to the transition here. The VRH to thermal activation transition behavior is often used to understand the breakdown of CES in many systems, including the conventional 2DEG [39], graphene [40], and more recently magnetic doped TI [2]. Nonlocal measurements are crucial for demonstrating the properties of CES as well. The temperature-dependent four-probe nonlocal resistance $R_{23/16}$ ($= V_{23}/I_{16}$) exhibits a similar behavior with the R_{xx} (see Fig. S5 in Supplemental Material [31]). The thermal activation gap of the nonlocal measurement from the Arrhenius fitting is $T_{nl} \sim 85$ K, which is roughly consistent with $T_0 \sim 92$ K. Due to the large bulk band gap (~200 meV) of $MnBi_2Te_4$ [7,18], the bulk carriers would not play a role in the temperature-dependent CES measurements. and it is the surface state carriers that contribute to the dissipative transport when temperature is increasing [19].

Meanwhile, the *B*-dependent sheet longitudinal resistance R_{sh} curves in regime I reveals a critical magnetic field (B_c). The four curves intersect at about –4.36 T [the inset of Fig. 3(e)]. In the vicinity of B_c, we plot the scaling behavior [41–44] of $\ln R_{sh} \sim \ln(|B–B_c|/T^{\kappa})$, as shown in Fig. 3(e). These curves would merge into one single curve, with the critical resistance being $\sim 1.2\,h/e^2$ and the exponent parameter $\kappa \sim 0.35$. The two parameters are similar to those seen in other systems, such as the transition from QAH state to Anderson insulator [41], the transition from axion insulator to Chern insulator [42], the quantum Hall plateau transition [44], and so on. It implies that the transition here also shares the same universality class [45].

The current (I)-dependent transport has also attracted significant interest, especially the current-induced breakdown of the quantization [24,27]. At 2 K, the values of R_{xx_min} in the quantization regime for different currents is shown in Fig. 3(f). We find that R_{xx_min} stays around 14 Ω when the current is less than 1.4 μA, and starts to increase obviously when $I > 1.4\,\mu$A. Thus, the critical current (I_C) for the breakdown of the quantization can be identified as 1.4 μA. The critical currents at different temperatures are plotted in Fig. 3(g), and

the value decreases with increasing temperature. Furthermore, I_C exhibits an almost linear relationship with temperature. Therefore, the effect of current on quantization may be similar to that of temperature. Two mechanisms can account for the current-induced breakdown of the dissipationless CES, i.e., electric-field-driven VRH [24] and bootstrap electron heating [25,27]. The breakdown that originates from bootstrap electron heating in QHE is often characterized by a large critical current (tens of μA), and there is usually an abrupt increase in the resistance [28,46,47]. However, the critical current for the Chern insulator state is relatively small ($\sim 1\mu$A) here, and an abrupt jump is not seen. Therefore, the current-induced breakdown cannot be explained by electron heating in this case. In our work, the current-induced breakdown resistance is a few tens of ohms [Fig. 3(f)], and it is as small as the R_{xx_min} in the VRH region in Fig. 3(a). The small breakdown resistance, together with the linear relationship between the critical current and the temperature, suggests that the electric-field-driven VRH is likely to be the origin. The area shaded orange in Fig. 3(g) roughly restricts the parameter space for the well-preserved dissipationless CES.

In another device (M6, see Fig. S7 in Supplemental Material [31] for more details), the effect of a *p-n* junction to the CES in Chern insulator is studied. Figure 4(a) is the configuration of the dual-gate device. A local top gate (V_{tg}), in addition to the back gate, is applied to form a *p-n* junction. At $B = 0$ T and $T = 1.7$ K, the dual gate mapping of $R_{16/16}$ is shown in Fig. 4(b). Guiding by the dashed lines, there are four quadrants according to the junction type, i.e. *p-n*, *p-p*, $n-p$, and *n-n*. Here the left letter represents the carrier type of the left part under top gate, and right one represents the right part of the device. In the Chern insulator state of M6, the $R_{16/16}$ and $R_{25/16}$ are plotted as a function of V_{tg} and V_{bg} [Figs. 4(c), 4(d)]. We find that the quantization exists in all the four regions. Figure 4(e) are line-cut profiles from Figs. 4(b)–4(d) with a certain V_{bg} of 33 V. Specifically, from the zero field $R_{16/16}$ [Fig. 4(e), top], it is in *p-n* region when $V_{tg} < -0.2$ V, and *n-n* region when $V_{tg} > -0.2$ V. $R_{25/16}$ [Fig. 4(e), bottom] is vanishingly small near $V_{tg} = -0.2$ V at 9T, and $R_{16/16}$ [Fig. 4(e), middle] is quantized to h/e^2 at the same time. This result means that a *p-n* junction would not affect the CES of the Chern insulator. In the QHE system with LL, a *p-n* junction would induce new plateaus, as reported in graphene [48,49]. Thus, it can be an important distinction between Chern insulator and QHE.

In summary, we realize the Chern insulator state in $MnBi_2Te_4$ devices with a well-defined Hall plateau maintained up to 22 K. The temperature- and current-dependent transport of the CES are studied systematically by both local and nonlocal measurements. An increase of temperature leads to three different regions, i.e., well-preserved dissipationless CES, VRH, and thermal activation. An increasing of current can induce the breakdown of the dissipationless CES, which is attributed to the electric-field-driven VRH. A *p-n* junction served as an extra dimension to modulate the CES provides meaningful insights. Our work forms a complete set of evidence and provide a comprehensive understanding on the Chern insulator state in $MnBi_2Te_4$.

We gratefully acknowledge the financial support of the National Key R&D Program of China (No. 2017YFA0303203), the National Natural Science Foundation of China (Grants No. U1732273, No. U1732159, No. 12025404, No. 12074181, No. 11904165, No. 11904166, No. 61822403, No. 11874203, No. 11834006, No. 91622115, No. 11522432, and No. 11574217), the Natural Science Foundation of Jiangsu Province (Grants No. BK20200007, No. BK20190286, No. BK20200312, and No. BK20200310), the Fundamental Research Funds for the Central Universities (No. 021314380147, No. 020414380149, No. 020414380150, No. 020414380151, No. 020414380192, and No. 020414380152), the Users with Excellence Project of Hefei Science Center CAS (No. 2019HSC-UE007), and the opening Project of the Wuhan National High Magnetic Field Center.

[1] F. D. M. Haldane, Phys. Rev. Lett. **61**, 2015 (1988).
[2] C.-Z. Chang, J. Zhang, X. Feng, J. Shen, Z. Zhang, M. Guo, K. Li, Y. Ou, P. Wei, L.-L. Wang, Z.-Q. Ji, Y. Feng, S. Ji, X. Chen, J. Jia, X. Dai, Z. Fang, S.-C. Zhang, K. He, Y. Wang, L. Lu, X.-C. Ma, and Q.-K. Xue, Science **340**, 167 (2013).
[3] M. Mogi, R. Yoshimi, A. Tsukazaki, K. Yasuda, Y. Kozuka, K. S. Takahashi, M. Kawasaki, and Y. Tokura, Appl. Phys. Lett. **107**, 182401 (2015).
[4] Y. Ou, C. Liu, G. Jiang, Y. Feng, D. Zhao, W. Wu, X.-X. Wang, W. Li, C. Song, L.-L. Wang, W. Wang, W. Wu, Y. Wang, K. He, X.-C. Ma, and Q.-K. Xue, Adv. Mater. **30**, 1703062 (2018).
[5] L. Pan, X. Liu, Q. L. He, A. Stern, G. Yin, X. Che, Q. Shao, P. Zhang, P. Deng, C.-Y. Yang, B. Casas, E. S. Choi, J. Xia, X. Kou, and K. L. Wang, Sci. Adv. **6**, eaaz3595 (2020).
[6] Y. Gong, J. Guo, J. Li, K. Zhu, M. Liao, X. Liu, Q. Zhang, L. Gu, L. Tang, X. Feng, D. Zhang, W. Li, C. Song, L. Wang, P. Yu, X. Chen, Y. Wang, H. Yao, W. Duan, Y. Xu, S.-C. Zhang, X. Ma, Q.-K. Xue, and K. He, Chin. Phys. Lett. **36**, 076801 (2019).
[7] M. M. Otrokov, I. I. Klimovskikh, H. Bentmann, D. Estyunin, A. Zeugner, Z. S. Aliev, S. Gaß, A. U. B. Wolter, A. V. Koroleva, A. M. Shikin, M. Blanco-Rey, M. Hoffmann, I. P. Rusinov, A. Y. Vyazovskaya, S. V. Eremeev, Y. M. Koroteev, V. M. Kuznetsov, F. Freyse, J. Sánchez-Barriga, I. R. Amiraslanov, M. B. Babanly, N. T. Mamedov, N. A. Abdullayev, V. N. Zverev, A. Alfonsov, V. Kataev, B. Büchner, E. F. Schwier, S. Kumar, A. Kimura, L. Petaccia, G. Di Santo, R. C. Vidal, S. Schatz, K. Kißner, M. Ünzelmann, C. H. Min, S. Moser, T. R. F. Peixoto, F. Reinert, A. Ernst, P. M. Echenique, A. Isaeva, and E. V. Chulkov, Nature (London) **576**, 416 (2019).
[8] D. Zhang, M. Shi, T. Zhu, D. Xing, H. Zhang, and J. Wang, Phys. Rev. Lett. **122**, 206401 (2019).
[9] J. Li, Y. Li, S. Du, Z. Wang, B.-L. Gu, S.-C. Zhang, K. He, W. Duan, and Y. Xu, Sci. Adv. **5**, eaaw5685 (2019).
[10] J. Q. Yan, Q. Zhang, T. Heitmann, Z. Huang, K. Y. Chen, J. G. Cheng, W. Wu, D. Vaknin, B. C. Sales, and R. J. McQueeney, Phys. Rev. Materials **3**, 064202 (2019).

[11] A. Zeugner, F. Nietschke, A. U. B. Wolter, S. Gaß, R. C. Vidal, T. R. F. Peixoto, D. Pohl, C. Damm, A. Lubk, R. Hentrich, S. K. Moser, C. Fornari, C. H. Min, S. Schatz, K. Kißner, M. Ünzelmann, M. Kaiser, F. Scaravaggi, B. Rellinghaus, K. Nielsch, C. Hess, B. Büchner, F. Reinert, H. Bentmann, O. Oeckler, T. Doert, M. Ruck, and A. Isaeva, Chem. Mater. **31**, 2795 (2019).

[12] M. M. Otrokov, I. P. Rusinov, M. Blanco-Rey, M. Hoffmann, A. Y. Vyazovskaya, S. V. Eremeev, A. Ernst, P. M. Echenique, A. Arnau, and E. V. Chulkov, Phys. Rev. Lett. **122**, 107202 (2019).

[13] B. Chen, F. Fei, D. Zhang, B. Zhang, W. Liu, S. Zhang, P. Wang, B. Wei, Y. Zhang, Z. Zuo, J. Guo, Q. Liu, Z. Wang, X. Wu, J. Zong, X. Xie, W. Chen, Z. Sun, S. Wang, Y. Zhang, M. Zhang, X. Wang, F. Song, H. Zhang, D. Shen, and B. Wang, Nat. Commun. **10**, 4469 (2019).

[14] C. Pei, Y. Xia, J. Wu, Y. Zhao, L. Gao, T. Ying, B. Gao, N. Li, W. Yang, D. Zhang, H. Gou, Y. Chen, H. Hosono, G. Li, and Y. Qi, Chin. Phys. Lett. **37**, 066401 (2020).

[15] J. Zhang, D. Wang, M. Shi, T. Zhu, H. Zhang, and J. Wang, Chin. Phys. Lett. **37**, 077304 (2020).

[16] W. Ko, M. Kolmer, J. Yan, A. D. Pham, M. Fu, F. Lüpke, S. Okamoto, Z. Gai, P. Ganesh, and A.-P. Li, Phys. Rev. B **102**, 115402 (2020).

[17] J. Q. Yan, S. Okamoto, M. A. McGuire, A. F. May, R. J. McQueeney, and B. C. Sales, Phys. Rev. B **100**, 104409 (2019).

[18] E. D. L. Rienks, S. Wimmer, J. Sánchez-Barriga, O. Caha, P. S. Mandal, J. Růžička, A. Ney, H. Steiner, V. V. Volobuev, H. Groiss, M. Albu, G. Kothleitner, J. Michalička, S. A. Khan, J. Minár, H. Ebert, G. Bauer, F. Freyse, A. Varykhalov, O. Rader, and G. Springholz, Nature (London) **576**, 423 (2019).

[19] Y. Deng, Y. Yu, Z. Shi Meng, Z. Guo, Z. Xu, J. Wang, H. C. Xian, and Y. Zhang, Science **367**, 895 (2020).

[20] D. Ovchinnikov, X. Huang, Z. Lin, Z. Fei, J. Cai, T. Song, M. He, Q. Jiang, C. Wang, H. Li, Y. Wang, Y. Wu, D. Xiao, J.-H. Chu, J. Yan, C.-Z. Chang, Y.-T. Cui, and X. Xu, Nano Lett. **21**, 2544 (2021).

[21] J. Ge, Y. Liu, J. Li, H. Li, T. Luo, Y. Wu, Y. Xu, and J. Wang, Natl. Sci. Rev. **7**, 1280 (2020).

[22] C. Liu, Y. Wang, H. Li, Y. Wu, Y. Li, J. Li, K. He, Y. Xu, J. Zhang, and Y. Wang, Nat. Mater. **19**, 522 (2020).

[23] D. G. Polyakov and B. I. Shklovskii, Phys. Rev. B **48**, 11167 (1993).

[24] M. Kawamura, R. Yoshimi, A. Tsukazaki, K. S. Takahashi, M. Kawasaki, and Y. Tokura, Phys. Rev. Lett. **119**, 016803 (2017).

[25] S. Komiyama and Y. Kawaguchi, Phys. Rev. B **61**, 2014 (2000).

[26] G. Nachtwei, Physica E **4**, 79 (1999).

[27] E. J. Fox, I. T. Rosen, Y. Yang, G. R. Jones, R. E. Elmquist, X. Kou, L. Pan, K. L. Wang, and D. Goldhaber-Gordon, Phys. Rev. B **98**, 075145 (2018).

[28] T. Okuno, S. Kawaji, T. Ohrui, T. Okamoto, Y. Kurata, and J. Sakai, J. Phys. Soc. Jpn. **64**, 1881 (1995).

[29] S. Zhang, R. Wang, X. Wang, B. Wei, B. Chen, H. Wang, G. Shi, F. Wang, B. Jia, Y. Ouyang, F. Xie, F. Fei, M. Zhang, X. Wang, D. Wu, X. Wan, F. Song, H. Zhang, and B. Wang, Nano Lett. **20**, 709 (2020).

[30] S. Yang, X. Xu, Y. Zhu, R. Niu, C. Xu, Y. Peng, X. Cheng, X. Jia, Y. Huang, X. Xu, J. Lu, and Y. Ye, Phys. Rev. X **11**, 011003 (2021).

[31] See Supplemental Material at http://link.aps.org/supplemental/10.1103/PhysRevB.105.085412 for methods, measurement details and additional transport data for devices in the main text and devices of thick $MnBi_2Te_4$ flakes.

[32] S. H. Lee, Y. Zhu, Y. Wang, L. Miao, T. Pillsbury, H. Yi, S. Kempinger, J. Hu, C. A. Heikes, P. Quarterman, W. Ratcliff, J. A. Borchers, H. Zhang, X. Ke, D. Graf, N. Alem, C.-Z. Chang, N. Samarth, and Z. Mao, Phys. Rev. Research **1**, 012011 (2019).

[33] A. J. Bestwick, E. J. Fox, X. Kou, L. Pan, K. L. Wang, and D. Goldhaber-Gordon, Phys. Rev. Lett. **114**, 187201 (2015).

[34] M. Büttiker, Phys. Rev. B **38**, 9375 (1988).

[35] J. G. Checkelsky, R. Yoshimi, A. Tsukazaki, K. S. Takahashi, Y. Kozuka, J. Falson, M. Kawasaki, and Y. Tokura, Nat. Phys. **10**, 731 (2014).

[36] D. E. Khmelnitskii, JETP Lett. **38**, 552 (1983).

[37] F. Hohls, U. Zeitler, and R. J. Haug, Phys. Rev. Lett. **88**, 036802 (2002).

[38] F. Xie, S. Zhang, Q. Liu, C. Xi, T.-T. Kang, R. Wang, B. Wei, X.-C. Pan, M. Zhang, F. Fei, X. Wang, L. Pi, G. L. Yu, B. Wang, and F. Song, Phys. Rev. B **99**, 081113 (2019).

[39] M. Furlan, Phys. Rev. B **57**, 14818 (1998).

[40] M. Yang, O. Couturaud, W. Desrat, C. Consejo, D. Kazazis, R. Yakimova, M. Syväjärvi, M. Goiran, J. Béard, P. Frings, M. Pierre, A. Cresti, W. Escoffier, and B. Jouault, Phys. Rev. Lett. **117**, 237702 (2016).

[41] C.-Z. Chang, W. Zhao, J. Li, J. K. Jain, C. Liu, J. S. Moodera, and M. H. W. Chan, Phys. Rev. Lett. **117**, 126802 (2016).

[42] X. Wu, D. Xiao, C.-Z. Chen, J. Sun, L. Zhang, M. H. W. Chan, N. Samarth, X. C. Xie, X. Lin, and C.-Z. Chang, Nat. Commun. **11**, 4532 (2020).

[43] C. Liu, Y. Ou, Y. Feng, G. Jiang, W. Wu, S. Li, Z. Cheng, K. He, X. Ma, Q. Xue, and Y. Wang, Phys. Rev. X **10**, 041063 (2020).

[44] D. Shahar, D. C. Tsui, M. Shayegan, R. N. Bhatt, and J. E. Cunningham, Phys. Rev. Lett. **74**, 4511 (1995).

[45] S. Kivelson, D.-H. Lee, and S.-C. Zhang, Phys. Rev. B **46**, 2223 (1992).

[46] G. Eber, K. v. Klitzing, K. Ploog, and G. Weinmann, J. Phys. C: Solid State Phys. **16**, 5441 (1983).

[47] M. E. Cage, R. F. Dziuba, B. F. Field, E. R. Williams, S. M. Girvin, A. C. Gossard, D. C. Tsui, and R. J. Wagner, Phys. Rev. Lett. **51**, 1374 (1983).

[48] J. R. Williams, L. DiCarlo, and C. M. Marcus, Science **317**, 638 (2007).

[49] D. A. Abanin and L. S. Levitov, Science **317**, 641 (2007).